

Title

Tree physiological monitoring of the 2018 larch budmoth outbreak: preference for leaf recovery and carbon storage over stem wood formation in *Larix decidua*

Authors

Richard L. Peters^{ab*}, Jose Carlos Miranda^{ac}, Leonie Schönbeck^a, Daniel Nievergelt^a, Marina V. Fonti^{ad}, Matthias Saurer^a, Ana Stritih^{ef}, Patrick Fonti^a, Beat Wermelinger^a, Georg von Arx^a, Marco M. Lehmann^a.

*Corresponding author: richard.peters@wsl.ch

Contact details

^aSwiss Federal Research Institute for Forest, Snow and Landscape Research (WSL), Zürcherstrasse 111, CH-8903 Birmensdorf, Switzerland

^bLaboratory of Plant Ecology, Department of Plants and Crops, Faculty of Bioscience Engineering, Ghent University, Coupure links 653, B-9000 Ghent, Belgium

^cForest Genetics and Ecophysiology Research Group, School of Forestry Engineering, Universidad Politécnica de Madrid, Ciudad Universitaria s/n, 28040, Madrid, Spain.

^dInstitute of Ecology and Geography, Siberian Federal University, 79 Svobodny pr., 660041 Krasnoyarsk, Russia

^eETH Zurich, Institute for Landscape and Spatial Development, Planning of Landscape and Urban Systems (PLUS), Stefano-Franscini Platz 5, 8093 Zürich, Switzerland

^fWSL Institute for Snow and Avalanche Research SLF, Flüelastrasse 11, 7260 Davos Dorf, Switzerland

Keywords

Insect outbreak, European Alps, *Zeiraphera griseana*, Wood formation, Non-structural carbohydrates (NSC), Stable Isotopes, Tree rings, Cell wall thickness

Word count

Abstract= 299, Introduction= 1509, Materials and methods= 1872, Results= 849, Discussion= 2340, Conclusion= 137.

Abstract

Insect defoliation impacts forest productivity worldwide, highlighting the relevance of plant-insect interactions. The larch budmoth (*Zeiraphera griseana* Hübner) is one of the most extensively studied defoliators, where numerous tree-ring based analyses on its host (*Larix decidua* Mill.) have aided in identifying outbreak dynamics over the past millennia. Yet, outbreaks have been widely absent after the early 1980s and little is known about the in situ tree-physiological responses and the allocation of carbon resources during and after defoliation.

In summer 2018, we tracked an on-going larch budmoth outbreak in a well-studied larch forest in the Swiss Alps. We performed bi-weekly monitoring on an affected and unaffected site using a unique combination of xylogenesis observations, measurements of non-structural carbohydrates (NSC), isotopic analysis of needle assimilates, and ground-based and remoted sensed leaf trait observations.

The budmoth induced a defoliation that lasted 40 days and could be detected by satellite observations. Soluble sugars significantly decreased in needles and stem phloem of the defoliated trees, while starch levels remained stable in the stem and root xylem compared to the control. Carbon and oxygen isotope ratios in needle assimilates indicated that neither photosynthetic assimilation rates nor stomatal conductance were different between sites before, during and after the outbreak. Defoliated trees ceased cell wall thickening 17 days earlier than unaffected trees, showing the earliest halt of ring formation recorded from 2007 till 2013 and causing significant thinner cell walls, particularly in the latewood. No significant differences were found for cell enlargement rates and ring width.

Our study revealed that an outbreak causes a downregulation of cell wall thickening first, while no starch is mobilized or leaf physiology is adjusted to compensate for the reduced carbon source due to defoliation. Our observations suggest that affected larch trees prioritize leaf recovery and carbon storage over wood biomass development.

Introduction

The evolutionary “arms race” between plants and insects has resulted in a wide variety of impacts on the host and subsequent plant-physiological adaptations (Pureswaran *et al.* 2018; Giron *et al.* 2018). Within forests, defoliating insects present a prominent biotic stressor that can negatively impact tree vitality and forest resilience to climate change (McDowell *et al.* 2008; Galiano *et al.* 2011; Poyatos *et al.* 2013; Anderegg *et al.* 2015; Foster 2017). The larch budmoth (*Zeiraphera griseana* Hübner) is such a defoliator, causing waves of extensive defoliation of its host, the European larch (*Larix decidua* Mill.), across the European alpine arch from West to East (Baltensweiler & Rubli 1999; Johnson *et al.* 2004). Such outbreaks have been part of these forest ecosystems for millennia, following ~9-year cycles (Baltensweiler & Fischlin 1988; Turchin *et al.* 2003; Esper *et al.* 2007). Yet, after the early 1980s they have been absent over most of the Alps, attributed to changes in forest structure, species composition or environmental conditions (e.g., Asshoff & Hättenschwiler 2006; Battipaglia *et al.* 2014; Johnson *et al.* 2010; Iyengar *et al.* 2016). However, it needs to be stressed that the population cycling continued with the same frequencies of minima and maxima as before, but without causing visible defoliation (Wermelinger *et al.* 2018). The missing outbreaks have halted further investigations of tree-physiological responses and adaptations to larch budmoth outbreaks. Remarkably, in 2016 a new outbreak wave, causing evident defoliation, started in France and reached western Switzerland in 2017. In 2018 widespread larch budmoth outbreaks were observed in several alpine valleys in Switzerland, which

provided a unique opportunity to study the direct tree-physiological response of *L. decidua* to larch budmoth larval feeding.

The larch tree - larch budmoth interactions are complex. During an outbreak, large quantities of larvae hatch in spring which feed on the needle clusters and cause visible defoliation. The host's crown foliage can be affected for up to 3 years after the first outbreak year (Baltensweiler & Rubli 1999; Baltensweiler *et al.* 2008). Larch is however not defenceless and responds by reducing foliage mass and nutritional quality for the defoliator (Benz 1974; Baltensweiler & Fischlin 1988; Asshoff & Hättenschwiler 2006). After a defoliation, larch is able to reflush its foliage within 3-4 weeks after the end of larval feeding, highlighting the resilience to this stressor (Baltensweiler *et al.* 2008). Such defoliations have most notably caused alterations of the wood structure, generating typical narrow annual tree rings with latewood tracheids showing thin latewood cell walls (Rolland *et al.* 2001; Esper *et al.* 2007). This impact on the wood structure is so severe and unambiguous that these "budmoth rings" have been commonly used to identify past outbreak events (Büntgen *et al.* 2009; Hartl-Meier *et al.* 2017; Arbellay *et al.* 2018). Moreover, in high-elevation forests these outbreaks show great relevance as they have a stronger impact on biomass accumulation than climate, with the absence of outbreaks since the 1980s causing substantial increases in growth rates (Peters *et al.* 2017; Weigt *et al.* 2017). Yet, the impact of defoliation by larch budmoth outbreaks on tree carbon dynamics depends on physiological responses of the host, which still are poorly understood (e.g., Medvigy *et al.* 2012).

Almost all knowledge on physiological responses to sudden defoliation comes from experimentally induced defoliations on small trees (but see Li *et al.* 2002), measuring the response in various plant organs. Remaining leaves appear to alter their functioning after a defoliation, i.e., artificially defoliated *Pinus radiata* (5-9 years old) compensated for foliage loss by temporarily increasing the photosynthetic capacity (Eyles *et al.* 2011; see also Reich 1992). Yet, the capability to alter photosynthetic performance appeared to be species specific (Gleason & Ares 2004; Piper & Fajardo 2014). For instance, for mature *L. decidua* oxygen ($\delta^{18}\text{O}$) and carbon isotopic ($\delta^{13}\text{C}$) ratios in tree rings during outbreaks occurring between 1900-2004 seemed largely unaffected (Kress *et al.* 2009; also found for *Abies balsamea* in Simard *et al.* 2012), suggesting similar stomatal conductance and photosynthetic capacity (see Scheidegger *et al.* 1999). Ambiguous results were also found for non-structural carbohydrates (NSC; including starch, sucrose, glucose and fructose) among different tree organs and species. Whilst 100% defoliation caused a significant depletion of NSC levels in roots of

treeline *Pinus cembra* (Li *et al.* 2002), studies on other species revealed only a short-term and limited impact on the NSC pools in different tree organs (e.g., needles, branches and roots; see Puri *et al.* 2015 studying *Pinus pinaster*), likely because trees prioritize carbon storage over structural carbon investment (Wiley *et al.* 2013; Jacquet *et al.* 2014). The removal of available carbon due to defoliation can also substantially down-regulate wood biomass formation (Schmid *et al.* 2017) and has severe implications for the wood structure, where defoliation can reduce xylem cavitation resistance, due to thinner and less lignified cell walls, and phloem transport efficiency, due to smaller and more irregular shaped phloem sieve tubes (Hillabrand *et al.* 2019). Among the few studies focussing on mature trees, Wiley *et al.* 2016 showed that defoliation strongly downregulates growth for 3 years while prioritizing re-foliation, NSC storage and maintaining the reproduction cycle (see also Puri *et al.* 2015). Unfortunately, these studies can only provide hypotheses about the potential regulating mechanisms, which have yet to be confirmed with in situ physiological measurement during a naturally occurring larch budmoth outbreak.

Defoliation after a larch budmoth outbreak requires *L. decidua* to invest carbon into building new foliage. The lower carbon availability during de- and re-foliation likely affects the formation of wood by the secondary meristem (the cambium) and the resulting wood structure. Budmoth rings are produced due to alterations in wood-formation kinetics, including duration and rate of cambial cell division, cell growth and cell-wall thickening (Cuny *et al.* 2014). Cell-wall thickening has been shown to have different kinetics than cell elongation (Cuny *et al.* 2015), yet is still impacted by the availability of NSC (Rathgeber *et al.* 2016; Friend *et al.* 2019). Moreover, wood-cell production and elongation, which determine ring width, are influenced by the turgor pressure in the cambium, hormone gradients, and the concentration of NSC (De Schepper & Steppe 2010; Simard *et al.* 2013; Hartmann *et al.* 2017). These wood-formation processes are likely hampered during a defoliation event and cause the production of fewer tracheids with thinner latewood cell walls, yet no wood formation observations are available to validate these assumptions. Thus, despite the fact that the resulting ring-width structure has been used for decades to reconstruct larch budmoth outbreak dynamics (e.g., Rolland *et al.* 2001), the underlying physiological mechanisms remain unclear.

Therefore, the question remains of how defoliation during a larch budmoth outbreak affects the physiology of the needles, and how this cascades to the NSC concentrations within different tree organs and subsequently affects the wood-formation processes. This short-term

reduction of carbon assimilation due to the defoliation is important as it alters the carbon input of mature trees growing under natural conditions (e.g., Rademacher *et al.* 2019). Based on these consideration we thus establish two contrasting hypotheses on the mechanism behind the observed reduction in secondary growth and its subsequent carbon allocation. One logical hypothesis (H1) is that the temporary lack of carbon, due to the reduced leaf area, is actively compensated by increasing photosynthetic capacity of the new foliage. The overcompensation stabilizes the NSC concentration in various tree organs to ensure long-term survival, while discriminating against wood formation processes (see Schmid *et al.* 2017). Conversely, (H2) leaf physiology of re-foliated needles stays unaltered, causing a lower availability of NSC concentrations in tree organs (e.g., twigs, stem and roots), and subsequently retards wood formation, as the lower availability of carbon resources reduces osmotic potential needed for turgor-driven cell elongation and resources to sustain cell wall thickening. This passive response would then show a subsequent reduction of NSC in storage tissues (e.g., stem xylem, root xylem) as these pools are not replenished (see Li *et al.* 2002).

Here we performed a unique bi-weekly physiological monitoring of mature *L. decidua* trees exposed to the first intense larch budmoth outbreak reported since the early 1980s. The study was conducted in a well-monitored high-elevation forest in the western Swiss Alps in 2018 (see King *et al.* 2013; Simard *et al.* 2013; Peters *et al.* 2019; Cuny *et al.* 2019), where weekly samples from multiple tissues (leaves, twig xylem, stem xylem, stem phloem and root xylem) were collected over the entire growing season on an affected and unaffected site. A unique combination of xylogenesis observations, NSC analysis, leaf trait measurements, and carbon and oxygen analyses were performed to track wood formation, carbon allocation dynamics, and leaf physiological performance. We expect H1 to be true, where the defoliation by the larch budmoth influences, i) the source-to-sink carbon allocation strategies, ii) the functionality of needles before and after the outbreak, and iii) the temporal dynamics of wood formation and wood anatomy. This study is among the first to perform multiple physiological measurements during an ongoing insect outbreak event and contributes to refining the understanding of mechanisms behind the impact of reduced carbon assimilation on tree physiology and wood production in mature trees.

Materials and Methods

Study site

The study area is located in the Lötschental valley of the Swiss Alps (46°23'40"N, 7°45'35"E; Figure 1a). The valley is largely covered by forest, composed of well-mixed

populations of Norway spruce and European larch, spanning from the valley bottom at 1300 m a.s.l. until 2200 m a.s.l. at the treeline (see Peters *et al.* 2017 for a detailed site description). In this valley at least 9 budmoth outbreaks occurred since 1900 (Peters *et al.* 2017; Büntgen *et al.* 2020). Mean annual total precipitation in the valley is 800 mm with mean annual air temperature of approximately 5 °C. The valley was selected due to the presence of outbreak and past intensive monitoring along an elevational transect (Simard *et al.* 2013; King *et al.* 2013; Peters *et al.* 2019). Particularly the data from a nearby site from Cuny *et al.* (2019) indicated as the “literature” site at 1900 m a.s.l. on the south facing slope in Figure 1a) was used to provide reference environmental measurements, wood formation monitoring and wood anatomical structure analyses spanning the period from 2007-2013. The site where the larch budmoth outbreak was observed (hence referred to as “budmoth site”) is located at the upper end of the optimal outbreak elevation (2000 m a.s.l.; Baltensweiler *et al.* 2008). A second site at a slightly lower elevation (1780 m a.s.l.; the “control site”) was established to provide a control under conditions not affected by budmoth outbreak. The mean age of mature *L. decidua* trees at these elevations is around 200 years (as reported by Peters *et al.* 2017 and Cuny *et al.* 2019). At both sites, air temperature (T_a) and relative humidity (RH) were monitored (using a Temperature/RH Sensor Data Logger with a temporal resolution of 10 minutes; Onset, USA, MX2302A; Figure 1b). The forest composition at both sites is similar, with *L. decidua* dominating (Figure 1c), while stand density and tree height was lower at the budmoth site (Table 1). At each site, four dominant and mature *L. decidua* trees were selected for continuous monitoring (Figure 1b). For each of the eight trees we recorded social status, position, height of the tree and its crown base (using a Vertex IV, Haglöf Sweden), and diameter at breast height (DBH; Figure 1c; Table 1).

Outbreak and sampling schedule

The sampling period started on the 20th June 2018 (DOY 171), when the larch budmoth outbreak was still at its early stage (i.e., limited visible feeding damage by young larvae; Table 2). Defoliation became clearly visible at the end of June (DOY 178) and reached its maximum at the beginning of July (DOY 186), with little difference in timing between trees. Re-foliation started in mid-July (DOY 193) and all buds were fully re-foliated at the end of July (DOY 209). At the beginning of August (DOY 217), only fully-grown mature needles were visible. Thus, the defoliation effect by the larch budmoth lasted for ca. 40 days (DOY 178 to 217). Further samples were taken until the end of the growing season on 10th October 2018 (DOY 283). All samples were consistently taken between 11:00 and 16:00 on each

sampling day. Additionally, on 9th August 2018 (DOY 221), one larger sun-exposed branch per tree was collected, where we randomly selected recent year twigs, transferred them to black plastic bags for transport, and stored them in the fridge in the laboratory for leaf trait analyses.

Sun-exposed needle and twig xylem samples were taken with a pole pruner at around 7 m height. Stem phloem (visually distinct from the xylem and dead bark due to a distinct coloration) and xylem (only sapwood) were collected with a 1 cm diameter increment borer (Haglöf, Sweden). Coarse root xylem was collected by digging out large accessible roots with a diameter of around 5-7 cm and chiselling out a 2×3 cm piece. Root sapwood samples were collected approximately once per month to minimize damage. All samples were transferred into gas-tight 12 ml glass vials (Exetainer, Labco, Lampeter, UK), stored in cooling bags with ice packs and afterwards frozen for NSC and stable isotope analyses. Afterwards, water was cryogenically extracted from needles and stem xylem using a vacuum-distillation line (Lehmann *et al.* 2018). Samples of twig xylem, stem phloem, stem xylem, and root xylem were oven-dried at 70 °C. All samples were ground to powder in a steel ball mill for further analysis.

In addition, microcores were collected at breast height on the stem using a Trephor (Rossi *et al.* 2006) and stored in ethanol to monitor xylogenesis at 4 to 17 days interval. At the end of the 2018 growing season a wood increment core was taken from each tree to analyse the wood anatomical structure.

Defoliation analyses and needle trait measurements

To track the defoliation patterns, we studied time series of satellite images and performed on-site evaluations of the needle traits and visually estimated defoliation of the crown area. We downloaded all cloud-free Sentinel-2 Level-2A (atmospherically corrected) images of the Lötschental for the growing seasons of 2017 and 2018 (European Space Agency, 2018). The NDVI (normalized difference vegetation index = $[\text{Near-infrared} - \text{Red}] / [\text{Near-infrared} + \text{Red}]$) of the study region was calculated at a 10-m resolution, and the mean value and standard deviation of pixels within the budmoth and control plots were extracted. To compare both sites while accounting for absolute productivity differences, we scaled the NDVI values to the maximum reached at each site during the growing season of 2017.

Needles from the whole branch sample (collected at DOY 221, so after full maturation of the new needles) were used to analyse needle leaf area (LA) using a leaf area meter (LI-

3100C, LI-COR, Lincoln, NE, USA). Dry weight (d.w.) of the needle material was determined after oven drying at 70 °C and needle length. The specific leaf area (SLA in m² kg⁻¹) is calculated as $SLA = LA/d.w.$. The carbon/nitrogen (C/N) ratio, before (DOY 171) and after (DOY 283) the larch budmoth outbreak was determined from 1 mg of weekly collected needle organic matter using an EA (EA1110 elemental analyser, CE Instruments, Milan, Italy) coupled to an IRMS (DeltaPlusXP, Thermo Fisher Scientific).

Analyses of non-structural carbohydrates (NSC)

NSC concentrations, reflecting low molecular weight sugars (glucose, fructose and sucrose) and starch, in needles, twig xylem, stem phloem, stem xylem and root xylem was determined using 10 to 12 mg of ground material, following the protocol as described in Schönbeck *et al.* (2018; see also Hoch *et al.* 2002). The total amount of soluble sugars was quantified photometrically at 340 nm in a 96-well microplate photometer (HR 7000, Hamilton, Reno, NE, USA) after enzymatic conversion to gluconate-6-phosphate (hexokinase reaction, hexokinase from Sigma Diagnostics, St. Louis, MO, USA). The total amount of NSC was determined by taking 500 µl of the extract (including sugars and starch) incubated (for 15 h at 49 °C) with a fungal amyloglucosidase from *Aspergillus niger* (Sigma-Aldrich, St. Louis, MO, USA) to digest starch into glucose and quantify the total amount photometrically. Pure starch and glucose-, fructose- and sucrose- solutions were used as standards, as well as leaf material with a known NSC concentration (Orchard leaves, Leco, St. Joseph, MI, USA). Soluble sugars and starch concentration values were standardized by dividing all values by their average per plot in the first sampling date ($[Ss_{std}]$ and $[St_{std}]$ respectively; see Table S1), in order to correct for absolute differences in NSC concentrations between sites before the outbreak and focus on differences in temporal dynamics.

Isotope analysis of source water and needle assimilates

The $\delta^{18}O$ of cryogenically extracted stem xylem water, as a proxy for source water, was analysed using a thermal combustion/elementary analysis (TC/EA) system coupled to a DeltaPlusXP isotope ratio mass spectrometer (IRMS; all supplied by Thermo Fisher Scientific, Bremen, Germany) with a typical measurement precision (*SD*) of 0.2‰.

For the extraction of assimilates, a total of 60 mg ground needle material was transferred to a 2 ml reaction tube, dissolved in 1.5 ml of hot (85 °C) water, and heated in a water bath at 85 °C for 30 min (Lehmann *et al.* 2017). Subsequently, samples were cooled

down at room temperature, centrifuged (2 min, 10000 g), and the supernatant containing the water-soluble compounds (WSC), was transferred to a new reaction vial. An aliquot (ca. 0.6 mg) of the WSC, as a proxy for assimilates, was transferred to silver capsules, frozen at -20 °C, and freeze-dried. Carbon ($\delta^{13}\text{C}$, VPDB) and oxygen ($\delta^{18}\text{O}$, VSMOW) isotope ratios were measured using a TC/EA system (vario PYRO cube, Elementar, Hanau, Germany) coupled to the above mentioned IRMS. The typical measurement precision (SD) was 0.3‰ for $\delta^{13}\text{C}$ values and 0.2‰ for $\delta^{18}\text{O}$ values. The ^{18}O -enrichment of needle assimilates ($\Delta^{18}\text{O}_{\text{WSC}}$) above source water was calculated as the difference between the $\delta^{18}\text{O}$ of WSC and the $\delta^{18}\text{O}$ of the stem xylem water (source water) in the same tree at the same date.

Xylogenes observations and wood anatomical measurements

Collected microcores were first embedded in paraffin and cut in 7 μm -thick transverse sections using a rotary microtome (Leica RM2245, Leica Biosystems, Nussloch, Germany). Sections were stained (with safranin and astra blue to distinguish cellulose and lignin) and permanently mounted on glass slides. Xylogenes observations were performed on the micro-sections using an optical microscope under visible and polarized light at $\times 100$ -400 magnification to distinguish the different phases of cell development (Rossi *et al.* 2006). Cambial, enlarging, cell wall thickening and mature cells were visually discriminated and counted for each sample according to Cuny *et al.* (2019). Count data of cells in different xylogenes phases were standardized by the total number of cells of the previous ring (Rossi *et al.* 2003) using the R package CAVIAR (Rathgeber *et al.* 2018). All xylogenes measurements were standardized (in %) to the total cells produced by the individual tree, to account for absolute cell production differences.

Additionally, quantitative wood anatomical analysis was used to determine cell-specific features and ring width using the increment core collected at the end of the monitoring period. For each slide, digital images were taken for the 2018 tree ring using a slide-scanner (Axio Scan Z1, Zeiss, Germany). ROXAS software (von Arx & Carrer 2014) combined with Image-Pro Plus (Media Cybernetics, Rockville, MD, USA), was used to measure tracheids semi-automatically from the images (von Arx *et al.* 2016). Cell lumen area and cell wall thickness, together with positional information (expressed in % of the 2018 tree ring), were measured to develop tracheidograms using the R package RAPTOR (Peters *et al.* 2018).

Statistics

Differences in the daily mean and amplitude of climatic conditions (T_a and RH) were tested using a paired student t-test. Linear mixed-effect models with treatment (“budmoth outbreak”), time (“seasonal variations”) and their interactions as fixed effects and the individual tree identification as random effect were used to test for significant differences in $[S_{std}]$, $[St_{std}]$, $\Delta^{18}O_{WSC}$, and $\delta^{13}C_{WSC}$. Differences in isotopic composition and in NSC between control and budmoth site at each sampling point were tested using a paired student t-test. For the xylogenesis and wood anatomical measurements, student’s t-tests were performed for each time step and cell position, respectively. The non-parametric Kruskal-Wallis test was used to examine differences between sites when there was a lack of residual normality and homogeneity. Statistical analyses were carried out using R version 3.5.1 (R Core Team 2018).

Results

Climate, crown structure and leaf trait differences

During the monitoring period no significant differences between sites were found in daily mean and amplitude of RH ($P = 0.15$ and 0.28 , respectively; Figure 1b). Mean daily T_a was slightly but significantly higher at the control site ($0.8\text{ }^{\circ}\text{C}$, $P < 0.01$), due to the higher difference in day and night time temperature at the outbreak site ($0.5\text{ }^{\circ}\text{C}$, $P = 0.01$). The mean daily temperature during the monitoring period (DOY 171-283) was relatively high compared to the period from 2007-2013 as reported by Cuny *et al.* (2019; $10.6 \pm 3.9\text{ }^{\circ}\text{C}$, see Figure S1), with 13.4 ± 3.4 and $12.6 \pm 3.5\text{ }^{\circ}\text{C}$ for the control and budmoth site, respectively. Satellite observations revealed the impact of the larch budmoth on the effective crown damage when comparing budmoth vs. control site (Figure 1d). Despite the moderate severity of the outbreak in the studied area (trees were not completely defoliated), re-foliated trees had lower NDVI after defoliation (from the second week of July on) compared to control trees, indicating lower leaf surface area and/or lower photosynthetic activity (Figure 1d). Compared to control plot, the new needles (collected at DOY 221) had a slightly larger surface and a markedly larger dry weight per needle, which resulted in a significantly lower SLA ($p = 0.03$; Table 3). No significant difference between sites was found for the C/N ratio of needles before and after defoliation ($P > 0.05$; results not shown).

Non-structural carbohydrates in different tissues

For all sampling dates and both sites, needles and stem phloem had the highest NSC (i.e., soluble sugars [Ss] and starch [St]) concentrations among all tissues (7.99% and 5.70%

dry weight for [Ss], and 2.49% and 10.36% d.w. for [St], respectively). Average NSC concentrations in xylem tissues were below 2% in d.w. (1.44%, 0.94% and 0.97% d.w. for [Ss], and 0.86%, 0.67% and 1.03% d.w. for [St] in twig, stem and root xylem, respectively). Standardized needle and stem phloem NSC concentrations [Ss_{std}] were significantly lower in defoliated trees after re-foliating, compared to control trees (Figure 2). Conversely, standardized stem xylem [Ss_{std}] was higher in damaged trees during re-foliation (DOY 193) and at the end of the season (DOY 283), compared to controls. Twig and root xylem did not show significant differences in [Ss_{std}] in control vs. defoliated trees. Starch [St_{std}] concentrations showed the most severe reduction in the needles of defoliated trees after re-foliation, and these minimum levels remained unchanged until the end of the growing season (significant except in DOY 239; Figure 2). However, [St_{std}] tended to increase in trees in twig xylem (significant in DOY 186, 283) and stem phloem (significant in DOY 239) in damaged trees. Stem and root xylem did not show differences between control and budmoth trees, nor did they change over time.

Seasonal carbon and oxygen isotopic composition in needle water and assimilates

The larch budmoth outbreak showed no clear effect ($P > 0.05$) on the carbon and oxygen isotopic composition of assimilates (WCS; Figure 3). However, clear seasonal variations of ca. 1‰ in $\delta^{13}C$ and 4.5‰ in $\delta^{18}O$ were observed ($P < 0.05$). Notably, differences in $\Delta^{18}O_{WSC}$ before the larch budmoth outbreak (DOY 171 and 172) are likely caused by strong day-to-day variations in atmospheric evaporative conditions (1.14 and 1.38 hPa for control and budmoth site, respectively).

Stem growth phenology and wood anatomy

The studied trees started cell enlargement before the sampling period, and stopped by DOY 209 (Figure 4). No significant difference was found between the dynamics of the relative enlarging cell count of the control and budmoth site ($P > 0.05$). Yet, compared to literature, the cell enlargement period ceased earlier than observed in the period from 2007-2013 (Figure 4). Cell wall thickening of the unaffected trees at the control site started between DOY 171 and 186, when defoliation was occurring at the budmoth site, while cell wall thickening ceased earlier than expected from literature data (Figure 4). Budmoth site trees ceased cell wall thickening 17 days earlier (DOY 251) than control trees (DOY 268). In addition, the number of cells that were still in the cell wall thickening phase was significantly

higher at the control site compared to the budmoth site at the end of the growing season (mean of DOY 239 and 251; $\Delta = 3$ cells when total cell production is around ~ 20 , $P = 0.015$).

Tree-ring width measured at 2018 showed no significant difference between the control and budmoth site ($P = 0.19$; Figure S2). When standardizing ring width to the previous year ring width, a non-significant reduction of 19% in ring width was found for the budmoth site ($P = 0.222$). The budmoth site appeared to have a slightly higher yet not-significant larger lumen area across the tree ring of 2018 (Figure 5). Although maximum cell lumen area remains unchanged between sites ($P = 0.717$), maximum cell wall thickness appears to be $1.24 \mu\text{m}$ lower for the budmoth site compared to the control site ($P = 0.052$). Budmoth trees showed overall thinner cell walls in 2018, with significant difference occurring in the latter part of the ring (66-76% of the tree ring; $P < 0.05$; Figure 5).

Discussion

Our multi-parameter physiological monitoring during the 2018 larch budmoth outbreak provides for the first time a physiological explanation for the altered stem wood structure of *Larix decidua*. Despite the fact that the monitored outbreak was not as extensive as past outbreaks (Baltensweiler & Rubli 1999; Baltensweiler *et al.* 2008; Wermelinger *et al.* 2018), it did reveal how insect defoliation impacts leaf physiology during and after the outbreak and how this cascades into carbohydrate storage and subsequently impacts wood formation.

Non-structural carbohydrate response to defoliation

The monitoring of the standardized seasonal non-structural carbohydrate (NSC) dynamics revealed that the trees growing at the outbreak site showed a significant differentiation from the control trees in relative soluble sugar levels in both needles and phloem after the outbreak (Figure 2). The lower starch and sugar concentrations in the needles of defoliated compared to control trees cascaded solely into a reduction of soluble sugars in the phloem but not in the stem or root xylem, which confirms previous studies that found a limited impact of defoliation on NSC pools due to a strong prioritization of carbon storage (Jacquet *et al.* 2014; Puri *et al.* 2015; Weber *et al.* 2019). Stem and root xylem NSC were not affected by defoliation in contrast to findings from Li *et al.* (2002), where carbon reserves were depleted in those tissues of evergreen *Pinus cembra* after defoliated. This could be due to the difference between deciduous *L. decidua* and evergreen conifers, which likely are better

adapted and have stricter control over their carbon storage pools due to the difference in the leaf economic spectrum (see Wright *et al.* 2004), where deciduous trees require more carbon for annual re-foliation. The trees at the outbreak site, however, showed a steeper increase in standardized starch concentrations in stem phloem and particularly in twig xylem compared to the control trees (Figure 2). Thus, NSC content in woody tissues remained generally unchanged or increased due to the budmoth outbreak, indicating that the affected trees prioritize maintenance of their NSC content and thus carbon availability after stress or that carbon pools are plentiful so that re-foliation does not affect previous NSC pools.

With normal seasonal patterns, sugars are increasingly made available within the cambium for cell wall thickening (as observed in *L. decidua* in Simard *et al.* 2013). Yet, the reduced carbon supply due to reduced leaf area and stable NSC content with prioritization for carbon storage in some tissues could explain the earlier halt of cell wall thickening in our study. The impact of lower carbon availability at the cambium has been studied by altering phloem transport, where the cut-off of sugars due to girdling had a strong down-regulating effect on cell wall thickness (shown in *Picea abies* in Winkler & Oberhuber 2017). These findings are also supported by artificial defoliation experiments (e.g., Wiley *et al.* 2016) which show that defoliation by the pine processionary moth on *Pinus nigra* tended to cause an increase in NSC concentrations while down-regulating growth (Palacio *et al.* 2012). For our high-elevation *L. decidua* trees, these results indicate that despite the availability of plentiful carbon for growth (as hypothesized by Körner 2003, contrasting Handa *et al.* 2005), the *L. decidua* trees prioritize re-foliation and the replenishment of their storage. The priority for carbon investment in re-foliation is likely enhanced as needles growing after defoliation have been shown to have a more carbon-demanding lignin content, supposedly as a defence against future herbivory (Asshoff & Hättenschwiler 2006). The priority for stored carbon could be an adaptation to the colder environmental conditions that require sugars within the stem (e.g., raffinose and pinitol) at the end of the growing season to facilitate the protection against frost-induced damages (Simard *et al.* 2013; Lintunen *et al.* 2016). In combination with previous findings, our results suggest a universal tree physiological response to various stressors like defoliation, cold temperatures or drought, where cambial activity and growth are strongly down-regulated during stress while attempting to maintain photosynthesis, storage and respiration (which was suggested for drought stress by McDowell 2011).

Absence of leaf physiological differences in regrown needles after budmoth outbreak

The unaltered ratio of C/N after defoliation agrees with Asshoff & Hättenschwiler (2006) who only found reductions in N the year after defoliation. Moreover, the specific leaf area was lower at the outbreak site (Table 3), suggesting that the trees produced more resource-intensive needles per unit leaf area. However, results from the carbon and oxygen isotope measurements of needle assimilates (Figure 3) did not provide clear evidence for a leaf functional response to the larch budmoth outbreak. Our results are therefore going along with isotope analyses of annual tree-rings on the same site (Kress *et al.* 2009), which also observed no clear influence of the larch budmoth outbreaks over several decades/centuries, although fluctuation in density and tree-ring growth were observed. The $\delta^{13}\text{C}$ and $\Delta^{18}\text{O}$ values in needle assimilates indicate that neither photosynthetic assimilation rates nor stomatal conductance were different between control needles and newly grown needles in budmoth affected trees (Scheidegger 2000). These results highlight that *L. decidua* does not increase photosynthetic capacity, as found in other species (e.g., Reich 1992; Eyles *et al.* 2011), emphasising the species-specific strategy of altering leaf physiology after a defoliation (Piper & Fajardo 2014). Moreover, the strong seasonality in $\Delta^{18}\text{O}$ values in assimilates in both treatments are explained by the changes in VPD during the growing season (Kahmen *et al.* 2011; Song *et al.* 2013), which was also previously observed at the same site in phloem organic matter (Treydte *et al.* 2014). This shows that the affected trees were able to maintain the physiological functionality of newly grown needles throughout the growing season, although environmental conditions during regrowth were different compared to those in spring (i.e., higher temperature and VPD) when the needles of control trees emerged.

Direct wood structural responses to the outbreak

Despite the fact that up to ~80% of the crown of the trees growing at the outbreak site was defoliated (Table 1), causing a reduction in the satellite derived NDVI (Figure 1d), no significant difference was found between the ring widths measured at the budmoth vs. control site (see Figure S2). These results contrast with past studies which successfully used ring width as a proxy for detecting defoliation events in the past, with narrow rings indicating an outbreak (Rolland *et al.* 2001; Büntgen *et al.* 2009; Hartl-Meier *et al.* 2017). We hypothesize that this discrepancy is present due to the timing of the outbreak, as maximum cell enlargement rates were already reached in this study causing a large part of the ring to be formed by the time the outbreak started (end of June; Figure 5). This is supported by the fact that 2018 was relatively warm (Figure S1) which is known to increase growth rates at these elevations and promote an earlier cambial onset (Frank & Esper 2005; Rossi *et al.* 2008; Cuny

et al. 2019). In addition, 2018 was an extremely dry year in Switzerland, with high temperatures and below-average precipitation in the spring and summer months (MeteoSchweiz 2018, Liechti *et al.* 2019). The effects of dry conditions likely explain the decrease in NDVI observed at both the control and budmoth sites in June, and could confound the differences between the budmoth and control sites. Alternatively, the impact of this particular outbreak on ring width could become more pronounced in the first years after the outbreak (see Baltensweiler *et al.* 2008; Peters *et al.* 2017), as the NSC reduction in the current year was not sufficient to reduce the osmotic pressure and subsequently reduce cambial division and cell enlargement, which is also driven by water availability (De Schepper & Steppe 2010; Cabon *et al.* 2019). Notwithstanding, the defoliation intensity of the outbreak could still have been moderate, as Baltensweiler & Rubli (1999) have reported events where defoliation occurred during multiple years. These findings question whether ring width is a proxy capable of detecting outbreak years of lesser intensity.

However, clear signs of the outbreak are recorded in the wood structure. The observations of wood formation revealed that cell wall thickening responded within the outbreak year, halting 17 days earlier at the budmoth compared to the control site, which is among the earliest occurrences of a stop of cell wall thickening monitored at the approximate elevation (Cuny *et al.* 2019; Figure 4). Additionally, the outbreak appeared to reduce the number of cells in the wall thickening phase after mid-August (DOY= 230; Figure 2), which resulted in significant thinner cell walls and thinner latewood at the budmoth site (Figure 5), characteristic for a budmoth ring (Rolland *et al.* 2001). The relatively early halt of enlargement and cell wall thickening at both sites in 2018 compared to previous observations (Cuny *et al.* 2019) could be attributed to the warm and dry conditions which is known to halt the wood formation processes (e.g., Vieira *et al.* 2014). Yet, the discrepancy in response of cell enlargement and wall thickening, where the budmoth site only differed in wall thickening, highlights the decoupling between radial growth and carbon allocation in cell walls (Cuny *et al.* 2015; Cuny *et al.* 2019). This discrepancy is also highlighted by the longer climatic response window of cell wall thickness compared to lumen diameter (as shown for climatic response of *Picea abies* in Castagneri *et al.* 2017). Notwithstanding, the fact that cell wall thickness responds within the year of outbreak confirms past studies, which detected outbreaks using latewood density and width (e.g., Esper *et al.* 2007; Arbellay *et al.* 2018). This observed hampering of carbon investment into thick cell walls is consistent with experimental studies, which showed a strong downregulation of carbon allocation in woody

biomass during defoliation (e.g., Schmid *et al.* 2017) and as a consequence could reduce mechanical stability (Hillabrand *et al.* 2019).

Is wood formation limited by carbon availability after the outbreak?

Our results present the first physiological monitoring of the intra-annual impact of a larch budmoth outbreak on the structure and function of *L. decidua*. We hypothesized that the temporal lack of carbon input due to defoliation would be compensated by either (H1) increasing photosynthetic capacity of the regrown needles, stabilizing NSC concentrations, while downregulating wood formation processes, or, in contrast, through (H2) an unaltered leaf physiology in regrown needles, reducing NSC levels and retarding wood formation. Our finding strongly supports the idea that needle growth and functioning is a high priority for larch budmoth affected trees, yet no alteration within the physiology of needles was observed, rejecting H1. We, however, only partially confirm H2, as *L. decidua* still seems to prioritize carbon storage over growth after a defoliation event, where starch levels are constant or increase in woody tissues throughout the season in budmoth affected trees. This reveals that NSC present within the trees is not the main factor regulating or limiting cambial activity (e.g., Hoch *et al.* 2002; Simard *et al.* 2013). The observed natural reduction in carbon availability due to defoliation and the subsequent response of internal carbon allocation reveal that there is a need to rethink the carbon source-sink paradigm (e.g., Friend *et al.* 2019), as there appears to be a stronger downregulation of wood formation processes while carbon is still available (Körner *et al.* 2015).

The absence of extensive budmoth outbreak after the early 1980s has prevented the detailed assessment of the physiological response of *L. decidua* to an outbreak. The absence of outbreaks has been attributed to changes in forest structure and species composition (Battipaglia *et al.* 2014; Hartl-Meier *et al.* 2017), changes in nitrogen, water, starch and sugar content of foliage (Turchin *et al.* 2003; Asshoff and Hättenschwiler, 2006) and climate (Johnson *et al.* 2010; Iyengar *et al.* 2016). The reason for its return in 2018 is unclear, yet the population growth dynamics of the budmoth appeared to continue its ~9 year cyclic pattern after the absence of visible defoliation events since the 1980s (e.g., Esper *et al.* 2007; Wermelinger *et al.* 2018; Büntgen *et al.* 2020). The pattern of lacking outbreaks and the recent resurrection occurred throughout the alpine arch, hinting towards the important role of large-scale climate effects in driving the budmoth population dynamics (Turchin *et al.* 2003). A recent study by Büntgen *et al.* (2020) attributes the reoccurrence to cold European winters

due to the persistent negative phase of the North Atlantic Oscillation, which they hypothesize to have caused a, i) reduction in egg mortality due to lower energy consumption through the extended diapause, ii) phenological synchrony between egg hatching and needle growth, and iii) shift of the outbreak epicentre to sub-alpine forests with higher host abundance. Due to the sudden return of the outbreak, we were unable to capture climatic conditions and wood formation dynamics at the start of the growing season, which could have provided more insights into the annual carbon allocation patterns. Additionally, monitoring of these multiple measurements should be continued to further explain lag effects on biomass accumulation, which have been observed up to 7 years after the outbreak (e.g., Peters *et al.* 2017). Although relative difference and seasonal dynamics of wood formation processes (i.e., cell enlargement and cell wall thickening) can be assessed (also due to the extensive reference dataset; Cuny *et al.* 2019), differences in absolute wood anatomical properties, carbon availability and growth might be influenced by differences in stand density (Table 1), tree size and local climatic conditions (Figure S1) between control and budmoth site. Additionally, while relative changes in NSC concentrations were assessed, it should be noted that absolute NSC concentrations are difficult to interpret due to difference in growing conditions between sites. Moreover, the high temperature and below average precipitation in summer of 2018 could have an interacting effect with defoliation on the wood structure, which is difficult to disentangle. Future and long-term investigations and experimental manipulations are thus needed to contribute to the better understanding of the interactions between insect outbreaks and internal carbohydrate allocation of trees and to assess the future fate of the forest sink capacity under changing outbreak regimes (e.g. Bale *et al.* 2002; McMahon *et al.* 2010; Medvigi *et al.* 2012).

Conclusion

Our study on the direct physiological response of subalpine *L. decidua* to a larch budmoth outbreak provides novel insights into the processes forming ring-width structures, which is important for a reliable reconstruction of outbreak dynamics over millennia. It sheds light on the process of tree carbon-allocation priorities in time of reduced carbon assimilation. Trees defoliated during a budmoth outbreak appeared to downregulate cell wall thickening, resulting in a wood structure with thinner cell walls and latewood, while not mobilizing longer-term starch storage or adjusting leaf physiology to increase carbon available for wood formation. These observations suggest that carbon dynamics and its storage have to be considered when assessing cambial activity and the subsequent carbon allocation into wood,

not only for insect outbreak events but potentially many other stressors, relevant for addressing the carbon sink capacity of forests.

Supplementary data

Supplementary data for this article is provided with the submission to *Tree Physiology*.

Acknowledgements

We thank Roman Zweifel for his aid in the field- and labwork performed at the Lötschental transect. We also would like to thank Andreas Rigling, Arthur Gessler, Flurin Babst and Stefan Klesse for discussion.

Conflict of interest

The authors declare that they have no conflict of interest.

Funding

The work supported by the Swiss National Science Foundation Early Postdoc.Mobility (grant P2BSP3_184475), LOTFOR (grant 150205), CLIMWOOD (grant 160077), and SNF Ambizione (grant PZ00P2_179978).

References

- Anderegg WRL, Hicke JA, Fisher RA, Allen CD, Aukema J, Bentz BJ, Hood S, Lichstein JW, Macalady K, McDowell NG, Pan Y, Raffa K, Sala A (2015) Tree mortality from drought, insects, and their interactions in a changing climate Research review Tree mortality from drought, insects, and their interactions in a. *New Phytologist* 208:674–683.
- Arbellay E, Jarvis I, Chavardès RD, Daniels LD, Stoffel M (2018) Tree-ring proxies of larch bud moth defoliation: Latewood width and blue intensity are more precise than tree-ring width. *Tree Physiology* 38:1237–1245.
- Asshoff R, Hättenschwiler S (2006) Changes in needle quality and larch bud moth performance in response to CO₂ enrichment and defoliation of treeline larches. *Ecological Entomology* 31:84–90.
- Bale JS, Masters GJ, Hodkinson ID, Awmack C, Bezemer TM, Brown VK, Butterfield J, Buse A, Coulson JC, Farrar J, Good JEG, Harrington R, Hartley S, Jones t H, Lindroth RL, Press MC, Symrnioudis I, Watt AD, Whittaker JB (2002) Herbivory in global climate change research: direct effects of rising temperature on insect herbivores. *Global Change Biology* 8:1–16.

- Baltensweiler W, Fischlin A (1988) The larch bud moth in the Alps. In: Berryman AA (ed) Dynamics of forest insect populations. Plenum Press, New York, pp 331-351.
- Baltensweiler W, Rubli D (1999) Dispersal: an important driving force of the cyclic population dynamics of the larch bud moth, *Zeiraphera diniana* Gn. Forest Snow and Landscape Research 74:1–153.
- Baltensweiler W, Weber UM, Cherubini P (2008) Tracing the influence of larch-bud-moth insect outbreaks and weather conditions on larch tree-ring growth in Engadine (Switzerland). Oikos 117:161–172.
- Battipaglia G, Büntgen U, McCloskey S, Blarquez O, Denis N, Paradis L, Brossier B, Fournier T, Carcaillet C (2014) Long-term effects of climate and land-use change on larch budmoth outbreaks in the French Alps. Climate Research 62:1–14.
- Büntgen U, Frank D, Liebhold A, Johnson D, Carrer M, Urbinati C, Grabner M, Nicolussi K, Levanić T, Esper J (2009) Three centuries of insect outbreaks across the European Alps. New Phytologist 182:929–941.
- Büntgen U, Liebhold A, Nievergelt D, Wermelinger B, Roques A, Reinig F, Krusic PJ, Piermattei A, Egli S, Cherubini P, Esper J (2020) Return of the moth: rethinking the effect of climate on insect outbreaks. Oecologia 192:543–552.
- Cabon A, Fernández-de-Uña, L Gea-Izquierdo G, Meinzer FC, Woodruff DR, Martínez-Vilalta J, De Cáceres M (2019) Water potential control of turgor-driven tracheid enlargement in Scots pine at its xeric distribution edge. New Phytologist.
- Castagneri D, Fonti P, Von Arx G, Carrer M (2017) How does climate influence xylem morphogenesis over the growing season? Insights from long-Term intra-ring anatomy in *Picea abies*. Annals of Botany 119:1011–1020.
- Cuny HE, Fonti P, Rathgeber CBK, von Arx G, Peters RL, Frank DC (2019) Couplings in cell differentiation kinetics mitigate air temperature influence on conifer wood anatomy. Plant Cell and Environment 42:1222–1232.
- Cuny HE, Rathgeber CBK, Frank D, Fonti P, Fournier M (2014) Kinetics of tracheid development explain conifer tree-ring structure. New Phytologist 203:1231–1241.
- Cuny HE, Rathgeber CBK, Frank D, Fonti P, Mäkinen H, Prislan P, Rossi S, del Castillo EM, Campelo F, Vavrčík H, Camarero JJ, Bryukhanova M V., Jyske T, Gričar J, Gryc V, De Luis M, Vieira J, Čufar K, Kirdyanov A V., Oberhuber W, Trembl V, Huang J-G, Li X, Swidrak I, Deslauriers A, Liang E, Nöjd P, Gruber A, Nabais C, Morin H, Krause C, King G, Fournier M (2015) Woody biomass production lags stem-girth increase by over one month in coniferous forests. Nature Plants 1:1–6.
- De Schepper V, Steppe K (2010) Development and verification of a water and sugar transport model using measured stem diameter variations. Journal of Experimental Botany 61:2083–2099.

- Esper J, Buntgen U, Frank DC, Nievergelt D, Liebhold A (2007) 1200 years of regular outbreaks in alpine insects. *Proceedings of the Royal Society B: Biological Sciences* 274:671–679.
- Eyles A, Smith D, Pinkard EA, Smith I, Corkrey R, Elms S, Beadle C, Mohammed C (2011) Photosynthetic responses of field-grown *Pinus radiata* trees to artificial and aphid-induced defoliation. *Tree Physiology* 31:592–603.
- Foster JR (2017) Xylem traits, leaf longevity and growth phenology predict growth and mortality response to defoliation in northern temperate forests. *Tree Physiology* 37:1151–1165.
- Frank D, Esper J (2005) Characterization and climate response patterns of a high-elevation, multi-species tree-ring network in the European Alps. *Dendrochronologia* 22:107–121.
- Friend AD, Eckes-Shephard AH, Fonti P, Rademacher TT, Rathgeber CBK, Richardson AD, Turton RH (2019) On the need to consider wood formation processes in global vegetation models and a suggested approach. *Annals of Forest Science* 76:49.
- Galiano L, Martínez-Vilalta J, Lloret F (2011) Carbon reserves and canopy defoliation determine the recovery of Scots pine 4yr after a drought episode. *New Phytologist* 190:750–759.
- Giron D, Dubreuil G, Bennett A, Dedeine F, Dicke M, Dyer LA, Erb M, Harris MO, Huguet E, Kaloshian I, Kawakita A, Lopez-Vaamonde C, Palmer TM, Petanidou T, Poulsen M, Sallé A, Simon JC, Terblanche JS, Thiéry D, Whiteman NK, Woods HA, Pincebourde S (2018) Promises and challenges in insect–plant interactions. *Entomologia Experimentalis et Applicata* 166:319–343.
- Gleason SM, Ares A (2004) Photosynthesis, carbohydrate storage and survival of a native and an introduced tree species in relation to light and defoliation. *Tree Physiology* 24:1087–1097.
- Handa IT, Körner C, Hättenschwiler S (2005) A test of the treeline carbon limitation hypothesis by in situ CO₂ enrichment and defoliation. *Ecology* 86:1288–1300.
- Hartl-Meier C, Esper J, Liebhold A, Konter O, Rothe A, Buntgen U (2017) Effects of host abundance on larch budmoth outbreaks in the European Alps. *Agricultural and Forest Entomology* 19:376–387.
- Hartmann F, Rathgeber C, Fournier M, Moulia B (2017) Modelling wood formation and structure: power and limits of a morphogenetic gradient in controlling xylem cell proliferation and growth. *Annals of Forest Science* 74:1–15.
- Hillabrand RM, Hacke UG, Lieffers VJ (2019) Defoliation constrains xylem and phloem functionality. *Tree Physiology* 39:1–29.
- Hoch G, Popp M, Körner C (2002) Altitudinal increase of mobile carbon pools in *Pinus cembra* suggests sink limitation of growth at the Swiss treeline. *Oikos* 3:361–374.

- Iyengar S V, Balakrishnan J, Kurths J (2016) Impact of climate change on larch budmoth cyclic outbreaks. *Scientific Reports* 6:27845.
- Jacquet JS, Bosc A, O'Grady A, Jactel H (2014) Combined effects of defoliation and water stress on pine growth and non-structural carbohydrates. *Tree Physiology* 34:367–376.
- Johnson DM, Buntgen U, Frank DC, Kausrud K, Haynes KJ, Liebhold AM, Esper J, Stenseth NC (2010) Climatic warming disrupts recurrent Alpine insect outbreaks. *Proceedings of the National Academy of Sciences* 107:20576–20581.
- Johnson DM, Bjørnstad ON, Liebhold AM (2004) Landscape geometry and travelling waves in the larch budmoth. *Ecology Letters* 7:967–974.
- Kahmen A, Sachse D, Arndt SK, Tu KP, Farrington H, Vitousek PM, Dawson TE (2011) Cellulose $\delta^{18}\text{O}$ is an index of leaf-to-air vapor pressure difference (VPD) in tropical plants. *Proceedings of the National Academy of Sciences of the United States of America* 108:1981–1986.
- King G, Fonti P, Nievergelt D, Buntgen U, Frank D (2013) Climatic drivers of hourly to yearly tree radius variations along a 6°C natural warming gradient. *Agricultural and Forest Meteorology* 168:36–46.
- Körner C (2015) Paradigm shift in plant growth control. *Plant Biology* 25:107–114.
- Körner C (2003) Carbon limitation in trees. *Journal of Ecology* 91:4–17.
- Kress A, Saurer M, Buntgen U, Treydte KS, Bugmann H, Siegwolf RTW (2009) Summer temperature dependency of larch budmoth outbreaks revealed by Alpine tree-ring isotope chronologies. *Oecologia* 160:353–365.
- Lehmann MM, Gamarra B, Kahmen A, Siegwolf RTW, Saurer M (2017) Oxygen isotope fractionations across individual leaf carbohydrates in grass and tree species. *Plant, Cell & Environment* 40:1658–1670.
- Lehmann MM, Goldsmith GR, Schmid L, Gessler A, Saurer M, Siegwolf RTW (2018) The effect of ^{18}O -labelled water vapour on the oxygen isotope ratio of water and assimilates in plants at high humidity. *New Phytologist* 217:105–116.
- Li M, Hoch G, Körner C (2002) Source/sink removal affects mobile carbohydrates in *Pinus cembra* at the Swiss treeline. *Trees - Structure and Function* 16:331–337.
- Liechti K., Barben M., Zappa M. (2019). Wasserhaushalt der Schweiz im Jahr 2018. Einordnung und Besonderheiten. *Wasser, Energie, Luft*, 111, 93–94.
- Lintunen A, Paljakka T, Jyske T, Peltoniemi M, Sterck F, Von Arx G, Cochard H, Copini P, Caldeira MC, Delzon S, Gebauer R, Grönlund L, Kiorapostolou N, Lechthaler S, Lobo-Do-Vale R, Peters RL, Petit G, Prendin AL, Salmon Y, Steppe K, Urban J, Juan SR, Robert EMR, Hölttä T (2016) Osmolality and non-structural carbohydrate composition in the secondary phloem of trees across a latitudinal gradient in Europe. *Frontiers in Plant Science* 7.

- McDowell N, Pockman WT, Allen CD, Breshears DD, Cobb N, Kolb T, Plaut J, Sperry J, West A, Williams DG, Yepez EA (2008) Mechanisms of Plant Survival and Mortality during Drought: Why Do Some Plants Survive while Others Succumb to Drought? *New Phytologist* 178:719–739.
- McDowell NG (2011) Mechanisms linking drought, hydraulics, carbon metabolism, and vegetation mortality. *Plant Physiology* 155:1051–1059.
- McMahon SM, Parker GG, Miller DR (2010) Evidence for a recent increase in forest growth. *Proceedings of the National Academy of Sciences* 107:3611–3615.
- Medvigy D, Clark KL, Skowronski NS, Schäfer KVR (2012) Simulated impacts of insect defoliation on forest carbon dynamics. *Environmental Research Letters* 7:45703.
- MeteoSchweiz 2018: Klimabulletin Sommer 2018. Zürich.
- Palacio S, Hernández R, Maestro-Martínez M, Camarero JJ (2012) Fast replenishment of initial carbon stores after defoliation by the pine processionary moth and its relationship to the re-growth ability of trees. *Trees - Structure and Function* 26:1627–1640.
- Peters RL, Balanzategui D, Hurley AG, von Arx G, Prendin AL, Cuny HE, Björklund J, Frank DC, Fonti P (2018) RAPTOR: Row and position tracheid organizer in R. *Dendrochronologia* 47:10–16.
- Peters RL, Speich M, Pappas C, Kahmen A, von Arx G, Graf Pannatier E, Steppe K, Treyde K, Stritih A, Fonti P (2019) Contrasting stomatal sensitivity to temperature and soil drought in mature alpine conifers. *Plant Cell and Environment* 42:1–16.
- Peters RL, Klesse S, Fonti P, Frank DC (2017) Contribution of climate vs. larch budmoth outbreaks in regulating biomass accumulation in high-elevation forests. *Forest Ecology and Management* 401:147–158.
- Piper FI, Fajardo A (2014) Foliar habit, tolerance to defoliation and their link to carbon and nitrogen storage. *Journal of Ecology* 102:1101–1111.
- Poyatos R, Aguadé D, Galiano L, Mencuccini M, Martínez-Vilalta J (2013) Drought-induced defoliation and long periods of near-zero gas exchange play a key role in accentuating metabolic decline of Scots pine. *New Phytologist* 200:388–401.
- Pureswaran DS, Roques A, Battisti A (2018) Forest insects and climate change. *Current Forestry Reports* 4:35–50.
- Puri E, Hoch G, Körner C (2015) Defoliation reduces growth but not carbon reserves in Mediterranean *Pinus pinaster* trees. *Trees* 29:1187–1196.
- Rademacher TT, Basler D, Eckes-Shephard AH, Fonti P, Friend AD, Le Moine J, Richardson AD (2019) Using Direct Phloem Transport Manipulation to Advance Understanding of Carbon Dynamics in Forest Trees. *Frontiers in Forests and Global Change* 2

- Rathgeber CBK, Cuny HE, Fonti P (2016) Biological Basis of Tree-Ring Formation: A Crash Course. *Frontiers in Plant Science* 7:1–7.
- Rathgeber CBK, Santenoise P, Cuny HE (2018) CAVIAR: an R package for checking, displaying and processing wood-formation-monitoring data. *Tree Physiology* 38: 1246–1260.
- Reich PB, Walters MB, Krause SC, Vanderklein DW, Raffe KF, Tabone T (1993) Growth, nutrition and gas exchange of *Pinus resinosa* following artificial defoliation. *Trees* 7:67–77.
- Rolland C, Baltensweiler W, Petitcolas V (2001) The potential for using *Larix decidua* ring widths in reconstructions of larch budmoth (*Zeiraphera diniana*) outbreak history: Dendrochronological estimates compared with insect surveys. *Trees - Structure and Function* 15:414–424.
- Rossi S, Deslauriers A, Morin H (2003) Application of the Gompertz equation for the study of xylem cell development. *Dendrochronologia* 21:33–39.
- Rossi S, Deslauriers A, Anfodillo T (2006) Assessment of Cambial Activity and Xylogenesis By Microsampling Tree Species: An Example At The Alpine Timberline. *IAWA Journal* 27:383–394.
- Rossi S, Deslauriers A, Grişar J, Seo JW, Rathgeber CBK, Anfodillo T, Morin H, Levanic T, Oven P, Jalkanen R (2008) Critical temperatures for xylogenesis in conifers of cold climates. *Global Ecology and Biogeography* 17:696–707.
- Scheidegger Y, Saurer M, Bahn M, Siegwolf R (2000) Linking stable oxygen and carbon isotopes with stomatal conductance and photosynthetic capacity: A conceptual model. *Oecologia* 125:350–357.
- Schmid S, Palacio S, Hoch G (2017) Growth reduction after defoliation is independent of CO₂ supply in deciduous and evergreen young oaks. *New Phytologist* 214:1479–1490.
- Schönbeck L, Gessler A, Hoch G, McDowell NG, Rigling A, Schaub M, Li MH (2018) Homeostatic levels of nonstructural carbohydrates after 13 yr of drought and irrigation in *Pinus sylvestris*. *New Phytologist* 219:1314–1324.
- Simard S, Giovannelli A, Treydte K, Traversi ML, King GM, Frank D, Fonti P (2013) Intra-annual dynamics of non-structural carbohydrates in the cambium of mature conifer trees reflects radial growth demands. *Tree Physiology* 33: 913–923.
- Simard S, Morin H, Krause C, Buhay WM, Treydte K (2012) Tree-ring widths and isotopes of artificially defoliated balsam firs: A simulation of spruce budworm outbreaks in Eastern Canada. *Environmental and Experimental Botany* 81:44–54.
- Song X, Barbour MM, Farquhar GD, Vann DR, Helliker BR (2013) Transpiration rate relates to within- and across-species variations in effective path length in a leaf water model of oxygen isotope enrichment. *Plant, Cell and Environment* 36:1338–1351.

- Treydte K, Boda S, Pannatier EG, Fonti P, Frank D, Ullrich B, Saurer M, Siegwolf R, Battipaglia G, Werner W, Gessler A (2014) Seasonal transfer of oxygen isotopes from precipitation and soil to the tree ring : source water versus needle water enrichment. *New Phytologist* 202:772–783.
- Turchin P, Wood SN, Ellner SP, Kendall BE, Murdoch WW, Fischlin A, Casas J, McCauley E, Briggs CJ (2003) Dynamical effects of plant quality and parasitism on larch budmoth. *Ecology* 84:1207–1214.
- Vieira J, Rossi S, Campelo F, Freitas H, Nabais C (2014) Xylogenesis of *Pinus pinaster* under a Mediterranean climate. *Annals of Forest Science* 71:71–80.
- von Arx G, Crivellaro A, Prendin AL, Čufar K, Carrer M (2016) Quantitative Wood Anatomy-Practical Guidelines. *Frontiers in Plant Science* 7:1–13.
- Weber R, Gessler A, Hoch G (2019) High carbon storage in carbon-limited trees. *New Phytologist* 222:171–182.
- Weigt RB, Streit K, Saurer M, Siegwolf RTW (2018) The influence of increasing temperature and CO₂ concentration on recent growth of old-growth larch: Contrasting responses at leaf and stem processes derived from tree-ring width and stable isotopes. *Tree Physiology* 38:706–720.
- Wermelinger B, Forster B, Nievergelt D (2018) Cycles and importance of the larch budmoth. *WSL Fact Sheet* 61:12.
- Wiley E, Casper BB, Helliker BR (2016) Recovery following defoliation involves shifts in allocation that favour storage and reproduction over radial growth in black oak. *Journal of Ecology* 105:412–424.
- Wiley E, Huepenbecker S, Casper BB, Helliker BR (2013) The effects of defoliation on carbon allocation: Can carbon limitation reduce growth in favour of storage? *Tree Physiology* 33:1216–1228.
- Winkler A, Oberhuber W (2017) Cambial response of Norway spruce to modified carbon availability by phloem girdling. *Tree Physiology* 37:1527–1535.

Figure legends

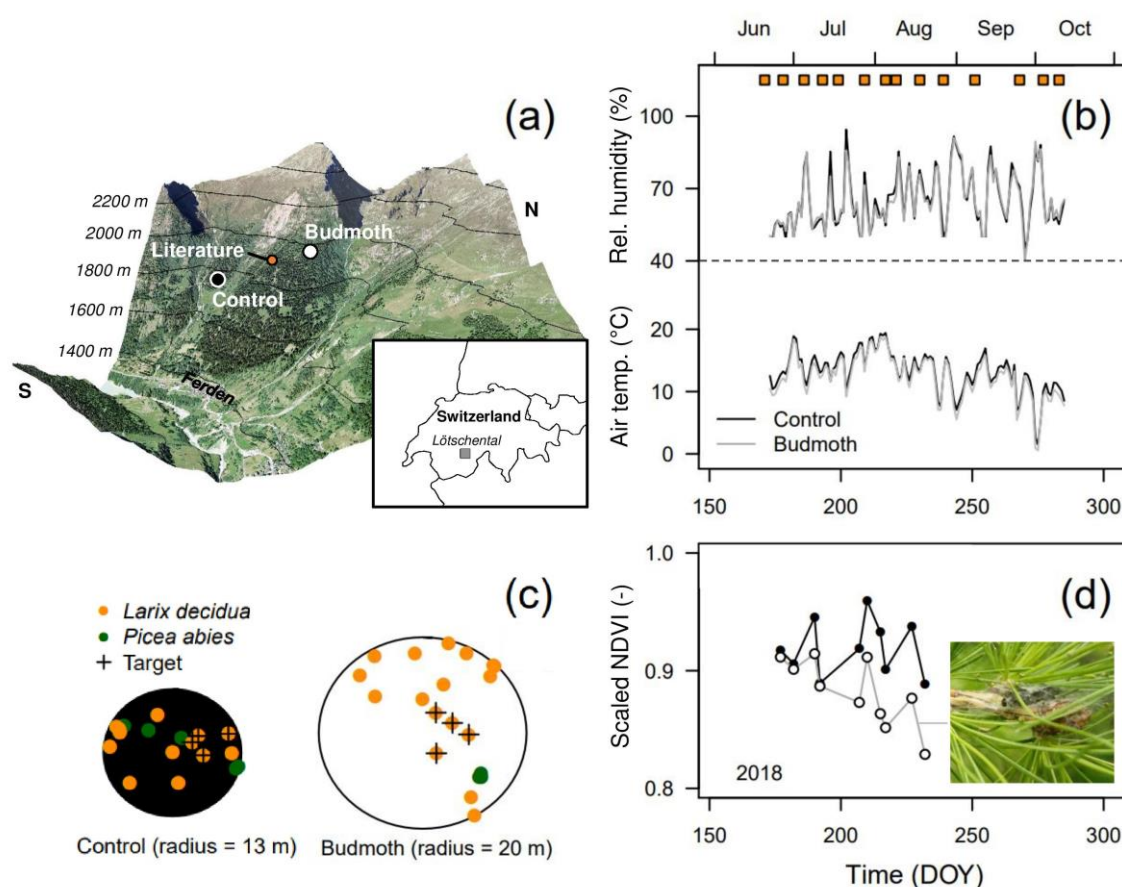


Figure 1. Sampling locations, experimental design and site characteristics. (a) Map of the Lötschental valley in Switzerland with an affected (budmoth; in white) and unaffected (control; in black) site from June to October. Additionally, data from literature on wood formation observation and wood anatomical information at a nearby site at 1900 m a.s.l., spanning the period from 2007-2013, was included (see Cuny *et al.* 2019; literature; in orange). (b) Daily mean relative humidity and air temperature time-series for the control (in black) and budmoth (in grey) site. Orange squares indicate the days of sampling. (c) Forest composition for both sites in a circular plot with a specified radius. Both *Larix decidua* and *Picea abies* trees are indicated, while the monitored *L. decidua* trees are highlighted (see Target). (d) The normalized difference vegetation index (NDVI) time series obtained from satellite images for 2018 (from July till August), scaled to the maximum NDVI value measured in the period from 2017 to 2018.

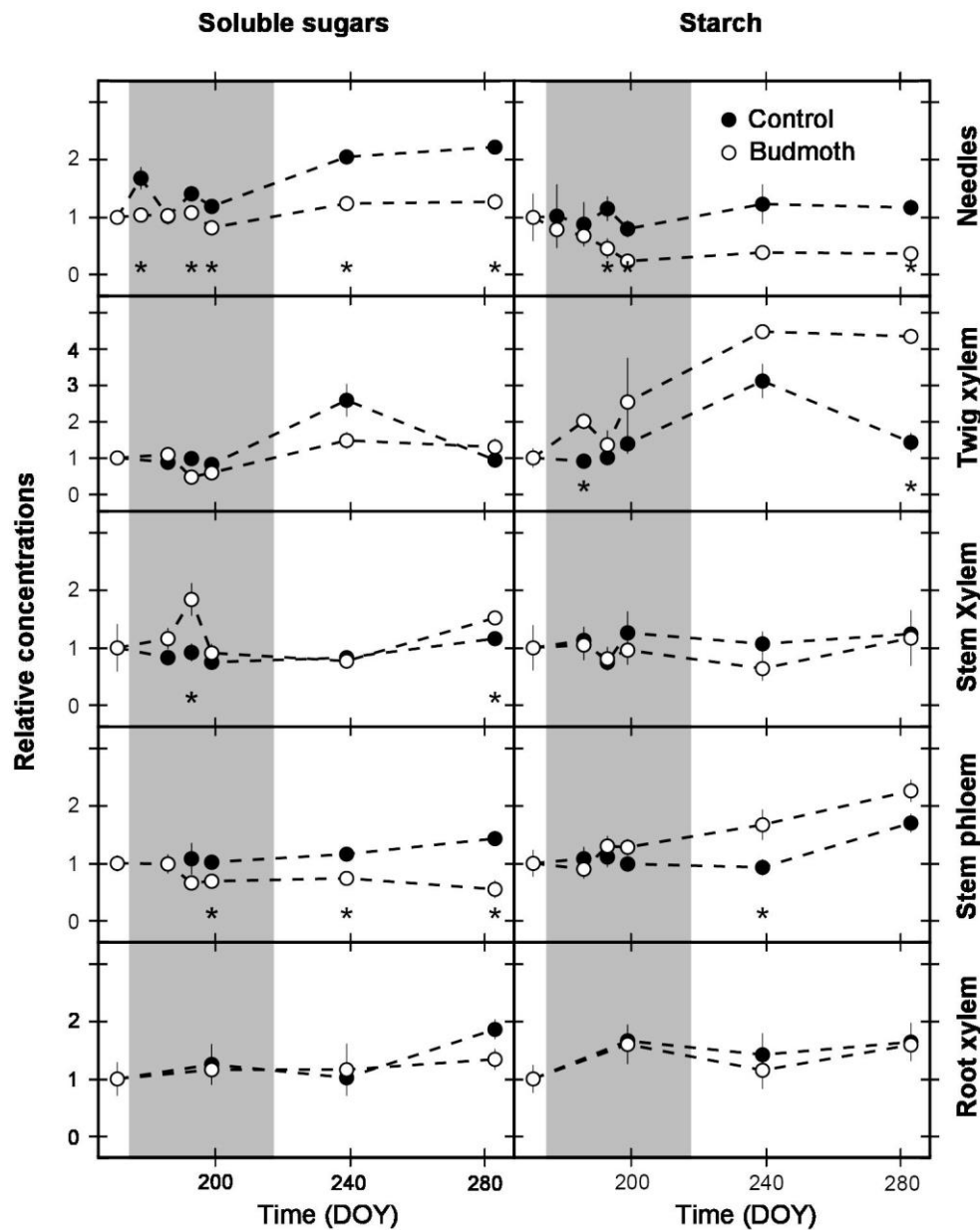


Figure 2. Seasonal non-structural carbohydrate (NSC) dynamics in different larch tree tissues. Standardized NSC concentrations of mean soluble sugar and starch content for different tissues of the control and budmoth site against the day of year (DOY) for the 2018 growing season. All NSC values were standardized by dividing by the tree-specific initial measurement taken on the 20th June 2018 (DOY 171). Stars (*) indicate significant differences between sites at that sampling date. The grey area reflects the period of visible larch budmoth defoliation. Mean values and standard errors are given (n = 4).

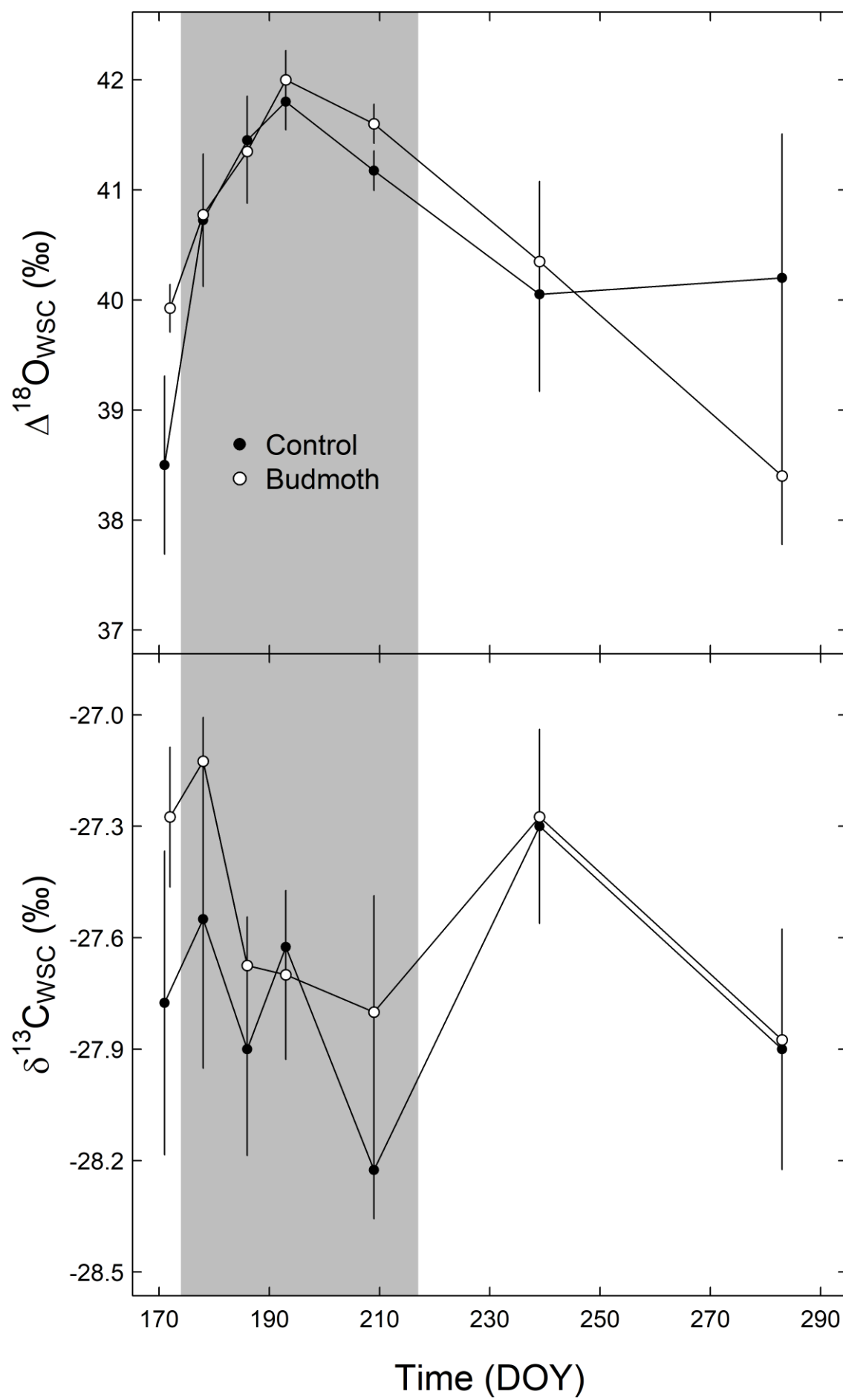


Figure 3. Seasonal isotope dynamics in larch needle assimilates carbon isotope ratios and oxygen isotope enrichment above source water for needle assimilates ($\delta^{13}\text{C}_{\text{WSC}}$ and $\Delta^{18}\text{O}_{\text{WSC}}$, respectively) from the control and budmoth site against the day of year (DOY) for the 2018 growing season. The grey area reflects the period of visible larch budmoth defoliation. Mean values and standard errors are given ($n = 4$).

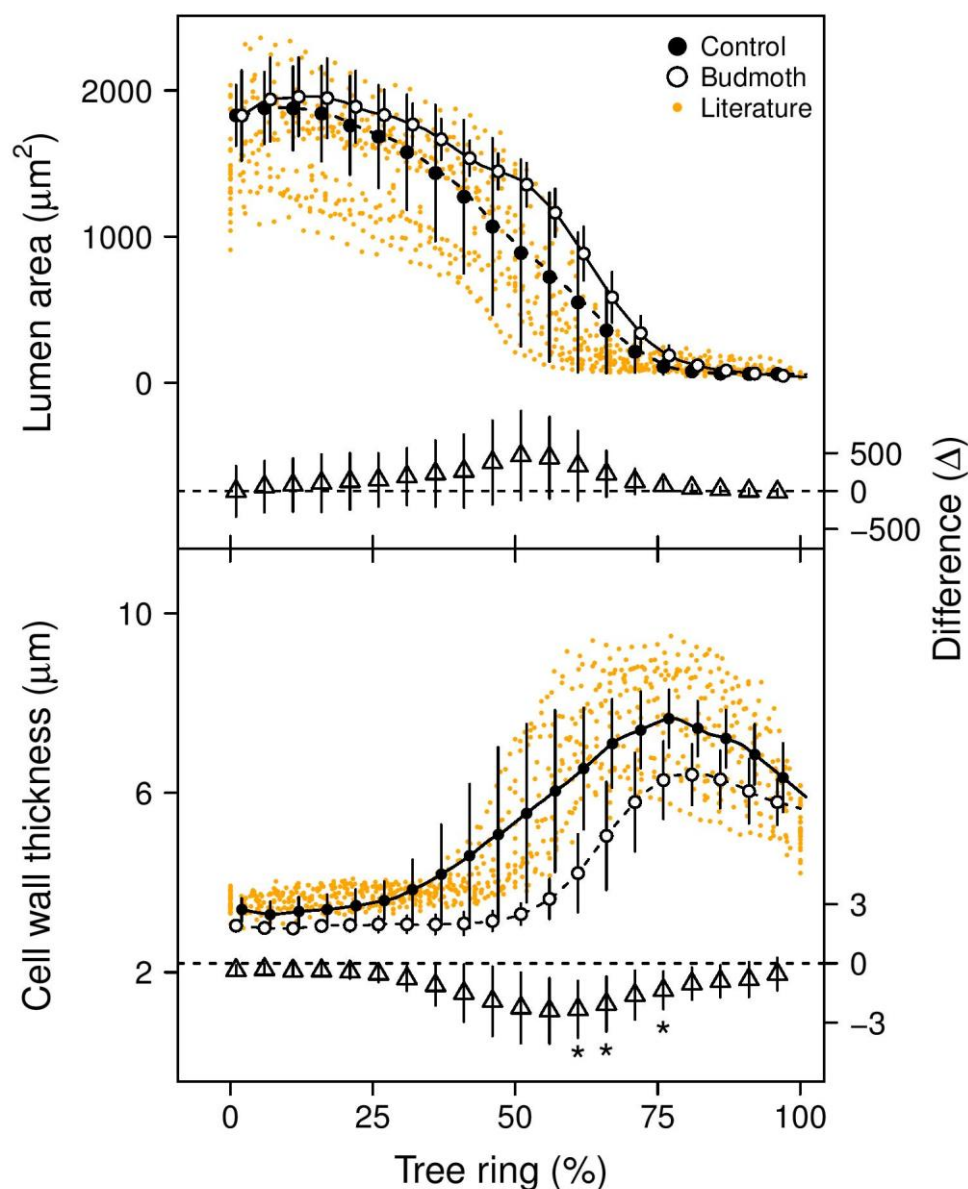


Figure 4. Relative cell count of tracheids in the enlarging (upper panel) and cell wall thickening (lower panel) phase against the day of year (DOY). Mean values and standard deviations are given ($n = 4$). Orange dots presents enlarging and cell wall thickening data

obtained from Cuny *et al.* (2019) for the period from 2007-2013 close to the monitoring sites. The general trend of these observations is highlighted with a cubic spline (orange bold line). Relative cell count is determined by standardizing the count data to the total amount of mature cells produced by the individual tree in the current year. The grey area reflects the period of larch budmoth defoliation. Stars (*) indicate significant differences between sites at that sampling date.

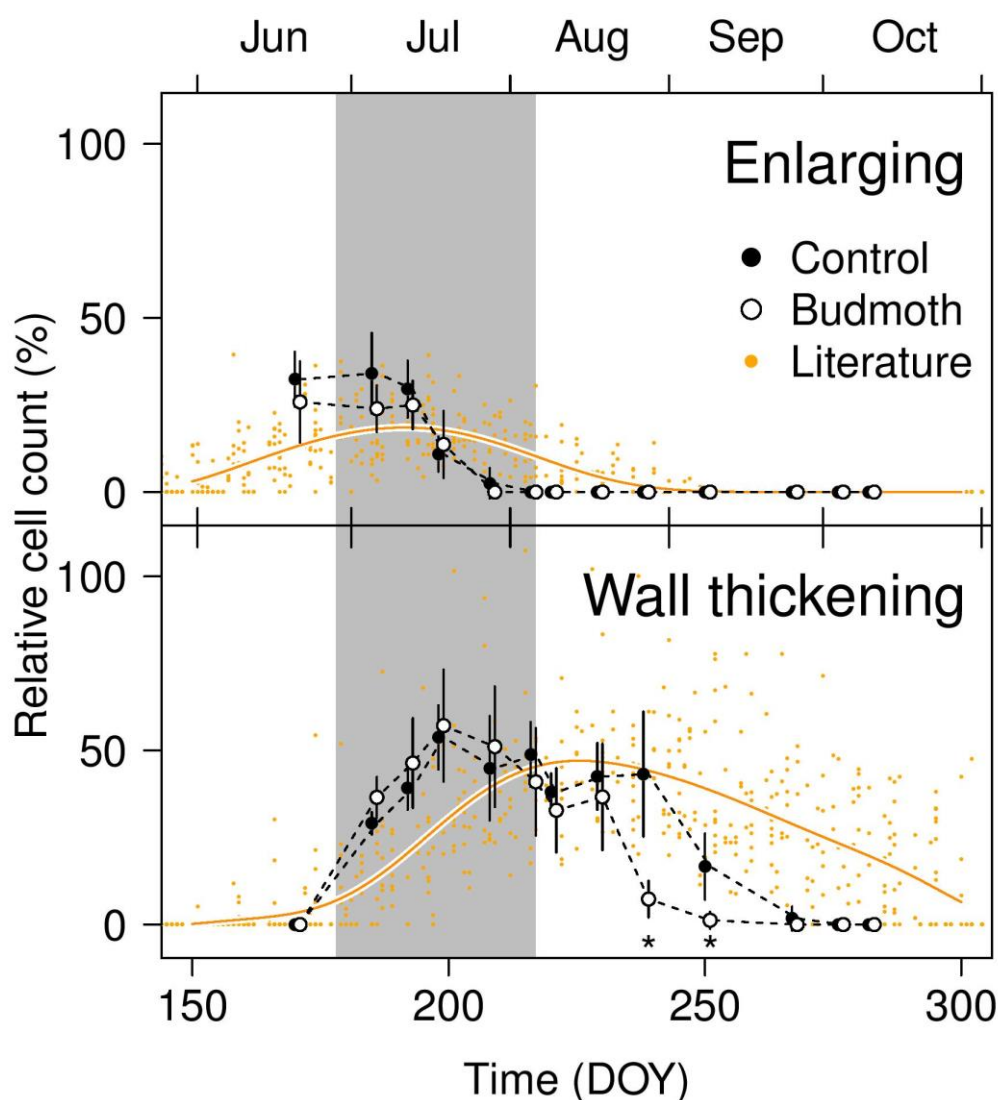


Figure 5. Lumen area and cell wall thickness composition in the 2018 tree ring of trees growing at the control and budmoth site. Orange dots presents lumen area and cell wall thickness data obtained from Cuny *et al.* (2019) for the period from 2007-2013 close to the monitoring sites. Data was standardized to the total cell count within 2018 of the individual

tree (tree ring in %). The difference axes indicate the differences between sites at that sampling date, stars (*) indicate significant differences. Mean and standard deviation are given (n = 4).

Table legends

Table 1. Main characteristics of sites and target trees.

Site	Lat. °N	Lon. °E	Elev. (m a.s.l.)	Stand density (tree ha ⁻¹)	Tree	DBH* (cm)	Height (m)	Crown base (m)	Defoliation (%)
Control	46.39475	7.74626	1780	339	C1	55	27.7	9.1	0
					C2	60	26.5	7.5	0
					C3	76.5	27.4	6.9	0
					C4	49.3	26.8	11	0
						60±12	27±1	9±2	
Budmoth	46.39922	7.74656	2000	167	D1	81.5	16.9	3.7	80
					D2	42.2	14.8	4	60
					D3	36.8	16.8	5	60
					D4	40.4	18.4	5.1	40
						50±21	17±2	5±1	

*DBH = Diameter at breast height (1.3 m)

Table 2. Outbreak and sampling schedule. For each tissue type the sampling day of year (DOY) is provided. The grey area indicates the period when trees showed visual damage from the outbreak.

Method	Tissue	DOY	June	July				August				September			
			171 [†]	178	186	193	199	209	217	221	230	239	251	268	277
XYL [*]	Stem xylem		X	X	X	X	X	X	X	X	X	X	X	X	X
NSC ^{**} /ISO ^{***}	Needles		X	X	X	X	X					X			X
NSC	Twig xylem														
NSC	Stem phloem		X		X	X	X					X			X
NSC/ISO	Stem xylem														
NSC	Root xylem		X				X					X			X
Budmoth damage				Defoliation	Max defoliation	Refoliating		Mature leaves							

*XYL = xylogenesis

**NSC = non-structural carbohydrates

***ISO = isotopic analyses of needle assimilates and stem xylem water

[†]The budmoth plot was first sampled on DOY 171 and control plot on DOY 172.

Table 3. Summary of various needle leaf traits of larch trees from the control and budmoth site (sampled on the 9th August 2018). Mean values and standard deviation (in brackets) are given (n = 4).

Site	Sampled total dry weight (mg)	Sampled total leaf area (cm ²)	Needle length (cm)	Specific Leaf Area (m ² kg ⁻¹)
------	----------------------------------	---	-----------------------	--

Control	46.8 (22.2)	7.9 (2.7)	2.1 (0.1)	17.6 (2.5)
Budmoth	82.3 (20.6)	10.7 (2.4)	2.3 (0.2)	13.2 (1.7)

UNCORRECTED MANUSCRIPT